ac susceptibility near the superconducting transition in polycrystalline $YBa_2Cu_3O_{7-\delta}$

W. M. Tiernan* and R. B. Hallock
Laboratory for Low Temperature Physics, Department of Physics and Astronomy, University of Massachusetts, Amherst, Massachusetts 01003
(Received 1 March 1993; revised manuscript received 8 November 1993)

We report temperature-dependent χ_{ac} measurements performed near the superconducting transition on three polycrystalline sintered $YBa_2Cu_3O_{7-\delta}$ samples for selected fixed magnetic fields $0.1 \leq H \leq 80.9$ G and ac excitation magnetic fields $0.9 \leq H_{ac} \leq 450$ mG. The nature of χ_{ac} was found to depend strongly on the magnitude of H_{ac} and for small H_{ac} we observe the breakdown of critical-state behavior. We estimate the threshold field for the critical state and interpret our results in the context of Josephson-array granular superconductivity.

I. INTRODUCTION

Sintered samples of $YBa_2Cu_3O_{7-\delta}$ (YBCO) consist of a matrix of small superconducting grains, and as a result exhibit two separate ac susceptibility (χ_{ac}) responses, one associated with intragranular superconducting currents and another associated with intergranular Josephson currents.[1,2] There have been many studies of intergranular χ_{ac} in sintered YBCO, and experimental χ_{ac} results are typically interpreted in the context of type-II superconductivity critical-state models.[3–6] A recent review article[7] discusses the current understanding of χ_{ac} and its relationship to J_c in both polycrystalline and single-crystal YBCO. Most χ_{ac} measurements on sintered YBCO are done with ac excitation fields $H_{ac} > 100$ milliGauss (mG). For smaller values of H_{ac}, superconducting critical-state models may not be applicable.[7,8] The regime of very small H_{ac} has not been investigated in sintered YBCO and the nature of intergranular χ_{ac} in this regime is not well understood. In this work we describe an extensive set of χ_{ac} measurements done on three YBCO sintered samples that investigate the evolution of χ_{ac} for small to moderate H_{ac}. These measurements were done for selected fixed magnetic field $0.1 \leq H \leq 80.9$ G, ac excitation fields $0.9 \leq H_{ac} \leq 450$ mG, and temperatures $80 \lesssim T \lesssim 93$ K.

II. BACKGROUND

The combination of grain boundary Josephson weak links and relatively large grain sizes that occur in sintered YBCO results in a material that provides an experimental realization of a Josephson-array granular superconductor.[9,10] The starting point for any Josephson-array model is the Josephson equations.[11,12] For a network of Josephson coupled grains, the Josephson current between grains i and j is $I_{ij} = I_{ij}^0 \sin(\theta_i - \theta_j - A_{ij})$. Here I_{ij}^0 is the Josephson critical current between grains i and j, θ_i is the superconducting phase of grain i, and A_{ij} depends on the vector potential $\mathbf{A}$ as

$$A_{ij} = (2\pi/\Phi_0) \int_i^j \mathbf{A} \cdot d\mathbf{r} \quad (1)$$

with $\Phi_0 = hc/2e$, the quantum of flux. Summing $A_{ij}/2\pi$ around a closed loop of grains gives the enclosed magnetic flux in units of the flux quantum Φ_0. The Josephson coupling energy between two grains is

$$E_{ij}^J = -(\hbar/2e) I_{ij}^0 \cos(\theta_i - \theta_j - A_{ij}) \; . \quad (2)$$

For a sintered YBCO sample, an experimentally measured critical-current density J_c is related to the average Josephson critical current $\langle I_{ij}^0 \rangle$, although a direct relationship is complicated by effects of thermal fluctuations and frustration. An applied magnetic field H produces A_{ij} terms and may reduce the I_{ij}^0. The reduction in I_{ij}^0 depends on the magnetic flux threading a single junction,[12] whereas the magnitude of A_{ij} terms depends on the magnetic flux enclosed by a closed loop of grains. For the measurements described here, we impose a fixed H and investigate the superconducting response as a function of the amplitude of the *ac* excitation field H_{ac}. H_{ac} is fairly small for all of our measurements, $H_{ac} < 0.5$ G, and for these values H_{ac} causes negligible reduction in the I_{ij}^0. Thus, the response to H_{ac} for our measurements can be attributed solely to changes in the A_{ij}.

The A_{ij} terms depend on the applied magnetic field, the sample morphology, and effects of shielding currents. The average grain size, the grain size distribution, and the percentage of the sample actually occupied by superconducting material all affect the relationship of the A_{ij} to the applied magnetic field H. The sample morphology sets a characteristic length scale l_g, which for reasonably dense samples should be comparable to the average grain size, $l_g \sim \langle d_g \rangle$. From Eq. (1), $\langle A_{ij} \rangle \approx (\pi/2) l_g^2 H/\Phi_0$, and l_g sets a magnetic field for frustration effects.[10] Frustration effects become important when $\langle A_{ij} \rangle \sim \pi/2$, so the characteristic frustration or "gauge glass" field is $H_g \sim \Phi_0/l_g^2$.

Screening currents complicate the relationship between H and $\langle A_{ij} \rangle$. There are two sources of screening; the partial Meissner effect from intragranular currents and bulk screening due to intergranular Josephson currents. Our samples were field cooled, and the extent of partial Meissner screening in individual grains depends on both the extent of flux pinning[13] and on the ratio of penetra-

tion depth to grain size $\lambda/\langle d_g \rangle$.[2,7] The volume of intragranular flux excluded can be estimated experimentally from χ' at large H_{ac}.[7] Two of our samples have $\langle d_g \rangle \sim 6$ μm, and for these flux exclusion is about 30–40% of the sample volume. One of the samples (1333) has $\langle d_g \rangle \sim 12$ μm, and the flux exclusion is about 60%. The importance of intergranular Josephson screening depends on the ratio of the Josephson penetration depth λ_J to both sample radius R and to the grain size. Most of our results are for the temperature region between T_{c0} and $T=80$ K. Here λ_J varies considerably, from $\lambda_J \gg R$ just below T_{c0} to $\lambda_J \sim \langle d_g \rangle$ for $T \approx 80$ K. Thus, intergranular shielding should be negligible just below T_{c0} but gain increasing importance with decreasing temperature.

Critical-state models may be applied to understanding intergranular currents in sintered YBCO if the measured response results from intergranular flux vortices moving over length scales larger than the grain size. Barriers to flux motion result in a gradient in the intergranular flux density, dB/dr, which, in turn, results in a critical-current density J_c. The critical-state model can be related to the Josephson array model as follows: If H_{ac} is large enough to produce changes $\langle \delta A_{ij} \rangle \sim \pi/2$, the system of Josephson coupled grains responds with collective rearrangements of the phases θ_i in order to minimize the system energy [see Eq. (2)]. This phase rearrangement is isomorphic to the motion of intergranular flux vortices across the sample, and potential wells and barriers encountered by moving integranular flux vortices correspond to minima and maxima of system energy for particular configurations of θ_i.[14] The applicability of critical-state models to Josephson-array systems requires that H_{ac} be greater than some threshold field H_{ac}^t. H_{ac}^t can be estimated in the context of the Josephson array model as H_{ac} which results in $\langle A_{ij} \rangle \sim \pi/2$. Notice that this condition is similar to that defining H_g, so that

$$H_{ac}^t \sim \Phi_0/l_g^2 \,. \tag{3}$$

III. APPARATUS AND TECHNIQUES

A closed-cycle refrigeration system[15] was used for the $\chi_{ac}(T)$ and $\rho(T)$ measurements described in this work and is described in Refs. 16 and 17. The sample block assembly was attached via a 13 mm×229 mm Cu connecting rod to the low-temperature stage of the closed-cycle refrigerator and temperature regulation was accomplished by a heater-temperature controller system. The cooling rate for temperature-dependent measurements was typically 0.3 mK/sec. Thermal contact between the sample and the sample block was made primarily at the current contacts and was quite good. For cooling rates $dT/dt \leq 1$ mK/sec we were unable to observe a difference between $\rho(T)$ for cooling as opposed to warming runs.

χ_{ac} measurements were performed by measuring changes in the mutual inductance between two solenoidal coils formed directly on the sample. These coils were fabricated on three ≈2mm×2mm×12.5mm sintered samples which were shaped to have a central region of approximately circular cross section for a length of ≈8mm. Since the samples are cylindrically shaped in the coil region and are considerably longer than the coils, they have negligible demagnetization factors. Figure 1(b) shows a sectional view along the length of a typical sample. Table I lists the mutual inductance L_{12} for the three samples described here. χ_{ac} is related to the emf $\mathcal{E}$ induced on the inner or secondary coil by the ac magnetic field H_{ac} produced by a sinusoidal current in the outer or primary coil, $\langle \mathcal{E} \rangle \propto (\omega/c)(1+4\pi\chi_{ac})\langle H_{ac} \rangle$. The in-phase $\mathcal{E}_X$ and quadrature $\mathcal{E}_Y$ components were measured with a two-phase lock-in amplifier and are related to the real (χ') and imaginary (χ'') parts of χ_{ac} as $\chi' = -(1/4\pi)(1-\mathcal{E}_X/\mathcal{E}_0)$ and $\chi'' = (1/4\pi)\mathcal{E}_Y/\mathcal{E}_0$. Here $\mathcal{E}_0$ is the induced emf above the superconducting transition. Figure 1(a) shows a schematic of the circuit used to perform χ_{ac} measurements. In these measurements the sinusoidal excitation field H_{ac} was superimposed on a fixed magnetic field H, with both H and H_{ac} applied parallel to the sample axis. Samples were field cooled, and $\chi(T)$ data were taken during cooling. H was produced by a 12-in. electromagnet and magnetic field was measured using a Hall effect gaussmeter. The vertical component of H between the pole pieces was less than 0.1 G.

The χ_{ac} measurements described here were done using a frequency $f=980$ Hz for H_{ac}. This frequency was chosen largely in order to provide an optimum signal at small H_{ac}. We also investigated the dependence of χ_{ac} on frequency for one of the samples (331) and found that χ'' is not significantly affected by changes in the frequency of H_{ac} in the range $17 \leq f \leq 3140$ Hz.[17]

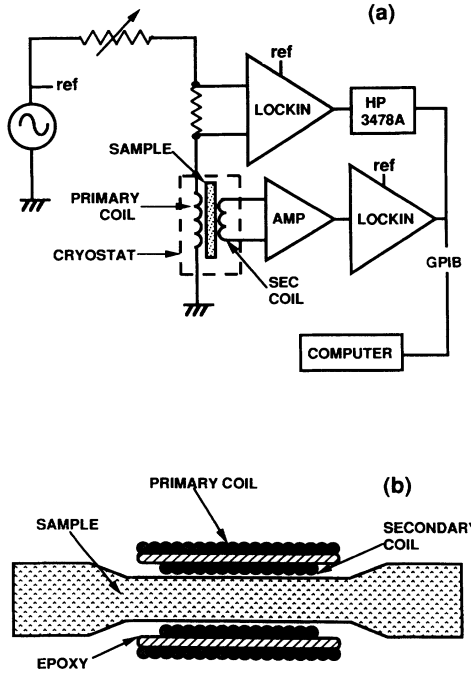

FIG. 1. (a) Schematic of circuit used for χ_{ac} measurements. (b) Sectional view along length of a typical sample.

TABLE I. Summary of physical characteristics measured for the three samples discussed in the text; density, average YBCO grain size, electrical resistivity at $T=300$ K, the single grain transition temperature T_{c0}, and the bulk superconducting transition temperature T_c. L_{12} gives the measured mutual inductance of a given χ_{ac} coil.

Sample	331	1765	1333
Density (g/cm^3)	5.4	5.1	5.4
$\langle d_g \rangle$ (μm)	5	6	12
ρ (300 K) (mΩ cm)	1.2	1.0	1.2
T_{c0} (K)	91.83	91.65	92.42
T_c (K)	90.83	90.50	
L_{12} (μH)	1.25	0.92	2.51

IV. MATERIALS SYNTHESIS AND CHARACTERIZATION

The three polycrystalline sintered samples described in this study were fabricated from YBCO powder made using the polymer-metal-complex precursor fabrication technique.[18–20] The powder was pressed into pellets, shaped, and then sintered at 940 °C. Table I summarizes several physical properties of the samples. The common features of $\approx 85\%$ sample density, room-temperature resistivity $\rho \approx 1$ mΩ cm, and superconducting transition widths $\delta T \approx 1$ K (Refs. 16 and 17) are all consistent with good quality sintered samples. The grain size distribution of the samples were analyzed from SEM images. A more complete description of sample synthesis and characterization is given in Refs. 16 and 17.

V. EXPERIMENTAL RESULTS AND DISCUSSION

A. General features of χ_{ac}

We first give a qualitative description of changes in χ' and χ'' as H_{ac} changes from very small values for which the critical-state picture is not applicable to larger values typically described by critical-state models. Figure 2 shows plots of χ' [Figs. 2(b), 2(d), and 2(f)] and χ'' [Figs. 2(a), 2(c), and 2(e)] for selected values of H_{ac} at fixed $H=0.5$ G for samples 331, 1765, and 1333, respectively. Figure 3 shows χ' [Figs. 3(b) and 3(d)] and χ'' [Figs. 3(a) and 3(c)] for sample 331 at selected values of H_{ac} at fixed $H=8.1$ and 80.9 G, respectively. It is obvious from these figures that χ_{ac} changes form as the magnitude of H_{ac} varies.

χ' is a measure of the shielding of H_{ac} by sample currents; for $\chi' \approx 0$ H_{ac} penetrates the sample freely, for $\chi' \approx -1/4\pi$ H_{ac} is completely screened at the surface of the sample. In all cases χ' has the general form of a step function, decreasing from zero below T_{c0}, falling relatively steeply, then leveling off at $\chi' \approx -1/4\pi$. In all of the samples there is a region just below T_{c0} for which χ' is independent of H_{ac} and falls roughly linearly with decreasing temperature. In this region $\chi'' \approx 0$. This is the region of very weak Josephson coupling where χ' is due solely to intragranular superconducting screening currents.

Lower temperatures produce stronger Josephson coupling, resulting in significant intergranular Josephson currents. Here χ'' is nonzero and the general form of both χ' and χ'' exhibits a complex dependence on the magnitude of H_{ac}. χ'' arises from currents that are out of phase with H_{ac} and is directly proportional to the energy dissipated per unit volume per cycle of H_{ac}.[21] For the values of H and H_{ac} used to obtain Figs. 2 and 3, χ'' arises virtually exclusively from intergranular Josephson currents. For all of the χ'' data shown in Figs. 2 and 3, as temperature decreases χ'' rises from zero to a maximum value and then falls again to zero, although the specific structure of this rise and fall depends on the magnitude of H_{ac}. For small H_{ac} ($\lesssim 9$ mG) the χ'' curves have distinctive and sample-dependent structure; for sample 331 χ'' has two distinct peaks, sample 1333 has a "shoulder" structure, and sample 1765 has a single peak. At larger H_{ac} ($\gtrsim 90$ mG) sample-dependent structure disappears and all samples have a similar χ'' structure, with a single peak and extended low-temperature "tail" as χ'' goes to zero. At large H_{ac} the width of the χ'' peak broadens and the peak position shifts to lower tempera-

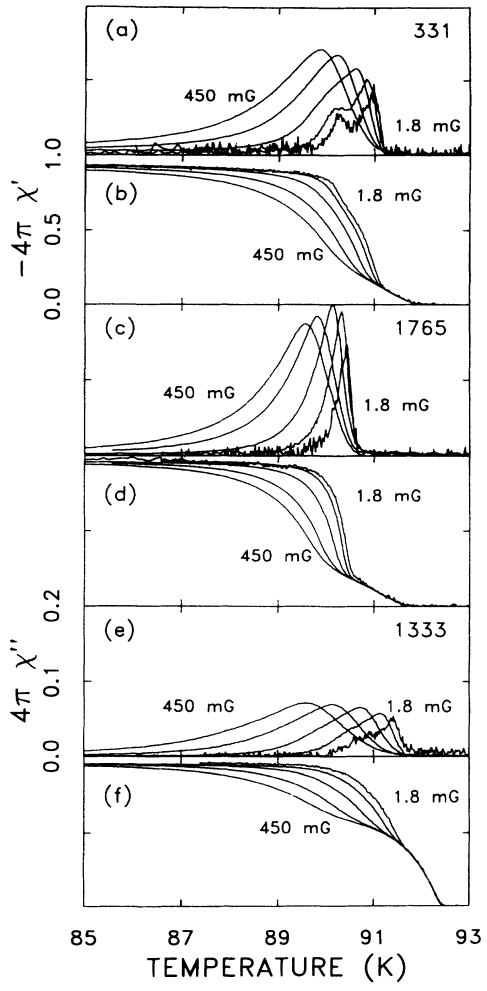

FIG. 2. χ' and χ'' vs T at selected $H_{ac}=1.8$, 9, 45, 180, and 450 mG and $H=0.5$ G. (a) χ'' for sample 331. (b) χ' for sample 331. (c) χ'' for sample 1765. (d) χ' for sample 1765. (e) χ'' for sample 1333. (f) χ' for sample 1333. The χ'' data [a, c, and e] have the same vertical scale and the χ' data [b, d, and f] have the same vertical scale.

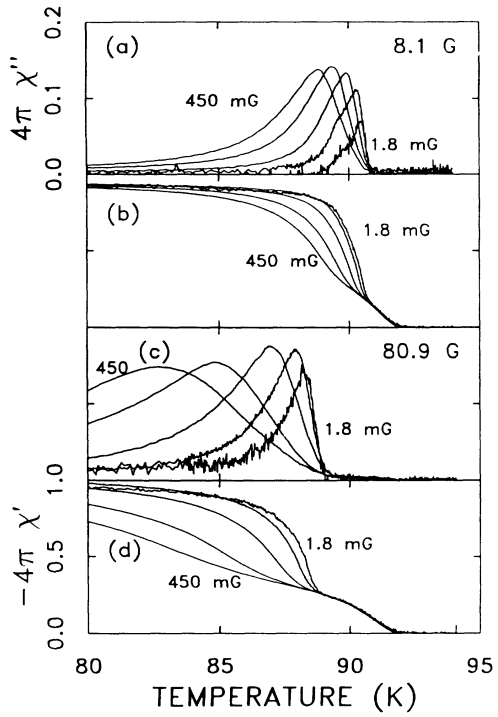

FIG. 3. χ' and χ'' vs T at selected $H_{ac}=1.8$, 9, 45, 180, and 450 mG for sample 331. (a) χ'' for $H=8.1$ G. (b) χ' for $H=8.1$ G. (c) χ'' for $H=80.9$ G. (d) χ' for $H=80.9$ G.

ture with increasing H_{ac}. The large H_{ac} behavior is similar to other experimental results that have successfully been analyzed using critical-state models.[7]

The extent and nature of superconducting screening can be inferred from χ' and χ''. The fraction of intragranular screening can be estimated from the limit of χ' for large H_{ac}. Thus, intergranular Josephson current screening can be determined at a given temperature from the difference between the value of χ' at the large H_{ac} limit and χ' for a given H_{ac}. For the smallest H_{ac}, intergranular currents cause rather abrupt changes in χ with decreasing temperature; at a sample-dependent temperature χ' drops steeply and χ'' increases steeply from 0. For small H_{ac} and $T\lesssim 89.5$ K, $\chi''\approx 0$, and the value of χ' reflects almost complete screening. These results are consistent with a reversible magnetization and a Josephson penetration depth $\lambda_J \ll R$ with R the sample radius.

The double-peak structure seen in sample 331 is a very different phenomenon from the χ'' double peak that has been reported for other samples at *large* H_{ac}. At large H_{ac} there may be two distinct χ'' peaks, one associated with intragranular response and a larger peak at lower temperature associated with intergranular response.[1] The double peak seen in sample 331, on the other hand, occurs at *small* H_{ac}, and both peaks are associated with intergranular Josephson currents. We are not aware of any previous observations of a solely intergranular χ'' double peak like that seen in sample 331.

Although the structure of χ' and χ'' varies considerably between samples and also as a function of H_{ac}, we observed an interesting correlation between χ' and χ''. For the temperature region in which χ_{ac} is determined by intergranular Josephson currents, it was found that the shape of $d\chi'/dT$ vs T was remarkably similar to that of χ'' vs T. This relationship between $d\chi'/dT$ and χ'' was observed for all samples and for all H_{ac}. Comparisons of $d\chi'/dT$ and χ'' are shown for sample 331 at $H=0.5$ G for $H_{ac}=9$ mG in Figs. 4(a) and 4(b) and for $H_{ac}=450$ mG in Figs. 4(c) and 4(d). For temperatures $T\lesssim 91$ K, χ_{ac} is due primarily to intergranular Josephson currents and the shape of $d\chi'/dT$ and χ'' agree very well. The double-peak structure in χ'' for $H_{ac}=9$ mG is visible in the $d\chi'/dT$ data. Although the shape of the two curves is very similar, the ratio of their magnitudes varies with H_{ac}. This variation largely reflects the broadening of χ' with increasing H_{ac}.

B. Strong Josephson coupling: χ'' dependence on H_{ac}

Figures 5–7 show the evolution of χ'' vs T for samples 331, 1765, and 1333 for fixed $H=0.5$ G as H_{ac} increases from 0.9 to 450 mG. Based on Figs. 5–7 and also Figs. 2 and 3, each sample has essentially three different regimes of χ'' behavior, depending on the magnitude of H_{ac}. For the smallest values of ac excitation magnetic field, $H_{ac}<9$ mG, χ'' as a function of T is nearly independent of H_{ac} for a given sample. Although independent of H_{ac}, the small H_{ac} χ'' curves do differ significantly among different samples. All of the samples share the following low H_{ac} features: (1) The peak value of χ'' is relatively small. (2) The shape of $\chi''(T)$ is relatively independent of H_{ac}. (3) The temperature of the χ'' peak changes little. (4) χ'' goes to zero with decreasing temperature in a well-defined fashion.

The behavior is different at larger excitation field. For $H_{ac}>90$ mG the general shape of $\chi''(T)$ is the same for all of the samples. Increasing H_{ac} noticeably shifts the

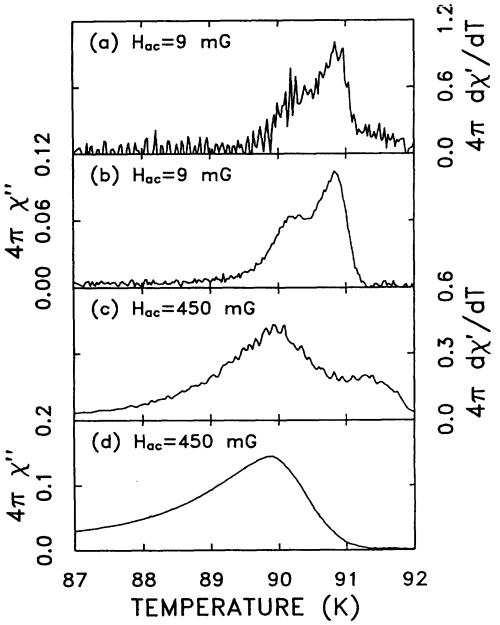

FIG. 4. $d\chi'/dT$ and χ'' vs T for sample 331 at $H=0.5$ G. (a) and (b) $H_{ac}=9$ mG. (c) and (d) $H_{ac}=450$ mG.

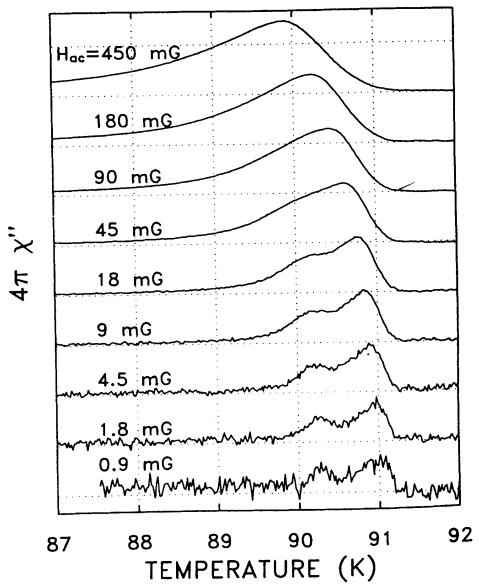

FIG. 5. χ'' vs T for sample 331 at $H=0.5$ G and selected values of H_{ac}. The separation between horizontal dotted lines corresponds to $4\pi\chi''=0.1$.

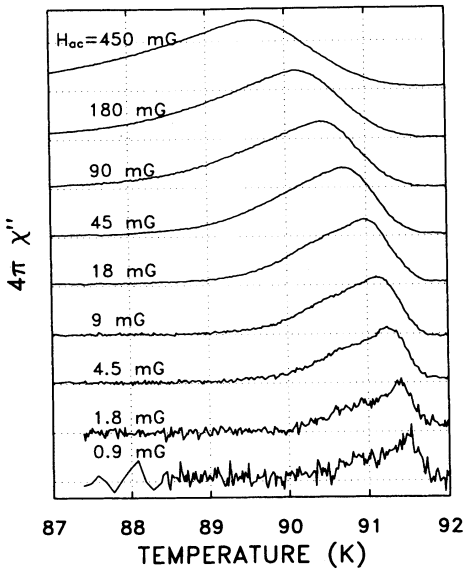

FIG. 7. χ'' vs T for sample 1333 at $H=0.5$ G and selected values of H_{ac}. The separation between horizontal dotted lines corresponds to $4\pi\chi''=0.05$.

peak of $\chi''(T)$ to lower temperature, broadens the $\chi''(T)$ peak, and produces an extended low-temperature "tail" that gradually approaches zero with decreasing temperature. This behavior is similar to that reported in other studies on sintered YBCO and explained in the context of critical-state models and the temperature dependence of J_c.[7]

The behavior at small H_{ac} is not consistent with critical-state models, suggesting that $H_{ac}<H_{ac}^{t}$. Moderate H_{ac}, for $9\lesssim H_{ac}\lesssim 90$ mG, is apparently a transition region between the two forms discussed above. Here, χ'' changes form; the peak value increases, the width broadens, and any structure apparent at lower H_{ac} gradually disappears with increasing H_{ac}. For the three samples we have estimated H_{ac}^{t} as the field for which small H_{ac} structure has disappeared and the peak value has shifted significantly. Using these criteria, we estimate $H_{ac}^{t}\approx 90$ mG for samples 331 and 1765, and $H_{ac}^{t}\approx 45$ mG for sample 1333. From Eq. (3), L_g can be estimated from H_{ac}^{t} as $l_g=\sqrt{\Phi_0/H_{ac}^{t}}$. For samples 331 and 1765 this gives $l_g\approx 15$ μm, which is over twice the average grain size of $\langle d_g\rangle\approx 6$ μm. For sample 1333, $l_g\approx 21$ μm, whereas $\langle d_g\rangle\approx 12$ μm. Thus, for all three samples $l_g\sim 2\langle d_g\rangle$.

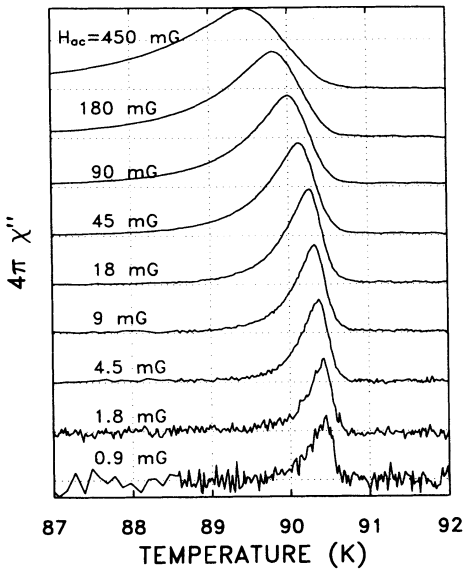

FIG. 6. χ'' vs T for sample 1765 at $H=0.5$ G and selected values of H_{ac}. The separation between horizontal dotted lines corresponds to $4\pi\chi''=0.1$.

For sample 331, changes in χ_{ac} as a function of changing the fixed magnetic field H in the range $0.1\le H\le 80.9$ G were also investigated. Comparison of Figs. 2(a), 3(a), and 3(c) shows that the double-peak structure of χ_{ac} occurring at small H_{ac} diminishes with increasing H and is not observable at $H=80.9$ G. Figures 8 and 9 show the evolution $\chi''(T)$ with increasing H for fixed $H_{ac}=1.8$ and 90 mG, respectively.

Other than for slight shifts in temperature, the structure of χ'' is not significantly affected by increasing H for $0.1\le H\le 2.0$ G. For $8\le H\le 80$, the peak value of χ'' at small H_{ac} appears to increase slightly. Based on these figures, the structure and H_{ac} dependence of χ'' is almost identical for $H\lesssim 2$ G, and shows increasing changes for $8.1\le H\le 80.9$ G. The shifts in position with increasing field can be partially attributed to the drop in T_c with increasing H. The evolving structure with increasing H also reflects the relatively strong H-dependent decrease in Josephson coupling for $H>5$ G.

C. Comparison with *I-V* measurements

We next compare our χ'' measurements with results from *I-V* isotherm measurements performed on samples

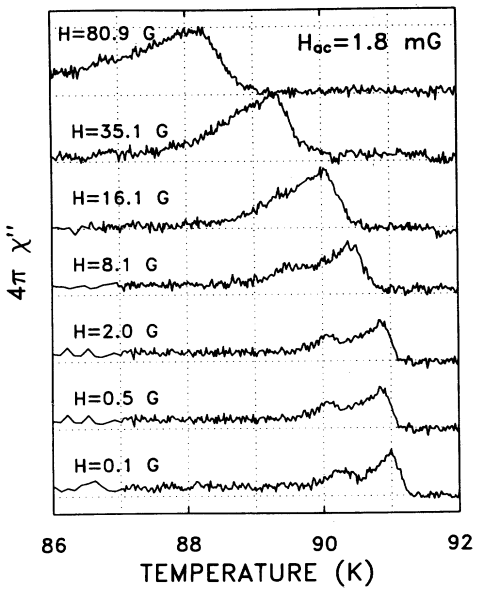

FIG. 8. χ'' vs T for sample 331 at fixed $H_{ac}=1.8$ mG and selected magnetic field $0.1 \leq H \leq 80.9$ G. Horizontal dotted lines are separated by $4\pi\chi''=0.1$.

331 and 1765 that are described in Refs. 16 and 17. For both of these samples we observed an evolution of nonlinear I-V characteristics consistent with recent predictions of I-V scaling near a superconducting transition. These measurements allowed a determination of a bulk superconducting transition temperature T_c. For sample 331, $T_c=90.83$ K and for sample 1765, $T_c=90.50$ K.

Above T_c both samples have ohmic I-V characteristics at low current densities, and in Ref. 16 we describe measurements of the sample resistivity ρ_L above T_c. $\rho_L \to 0$ as $T \to T_c$, and the initial increase in χ'' occurs near $\rho_L \to 0$. Thus, for $T > T_c$ and small H_{ac}, χ'' should be

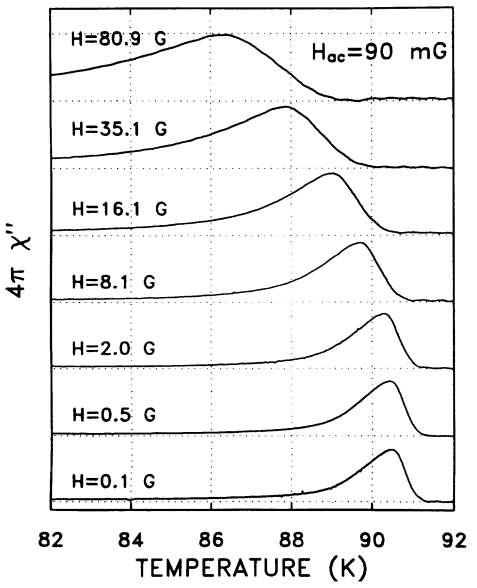

FIG. 9. χ'' vs T for sample 331 at fixed $H_{ac}=90$ mG and selected magnetic field $0.1 \leq H \leq 80.9$ G. Horizontal dotted lines are separated by $4\pi\chi''=0.1$.

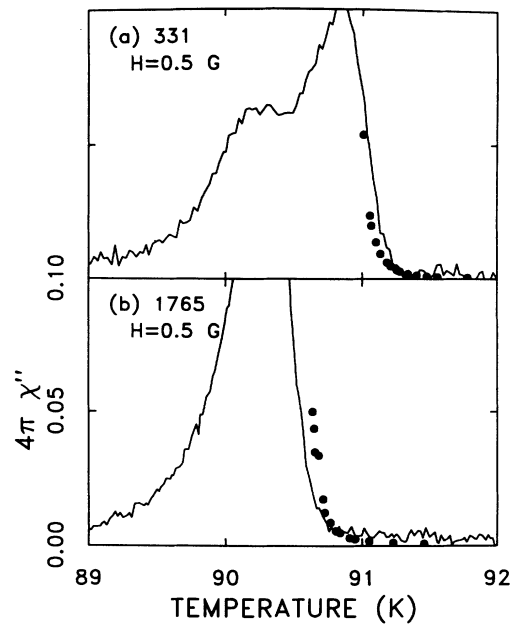

FIG. 10. χ'' vs T as measured directly (solid line) and as calculated (symbols) from ρ_L measurements. (a) Sample 331 and $H=0.5$ G. (b) Sample 1765 and $H=0.5$ G. The vertical scales are the same in (a) and (b).

consistent with a normal metal skin depth effect. For small screening currents, so that $4\pi\chi'' \ll 1$ and $\chi' \approx 0$, a normal metal skin depth approximation gives[21]

$$4\pi\chi'' \approx \mu_0 \omega R^2/8\rho \ . \tag{4}$$

Here ρ is the sample resistivity and R is the sample radius. Figures 10 and 11 show a comparison of χ'' measured directly with that calculated using Eq. (4) and ρ_L

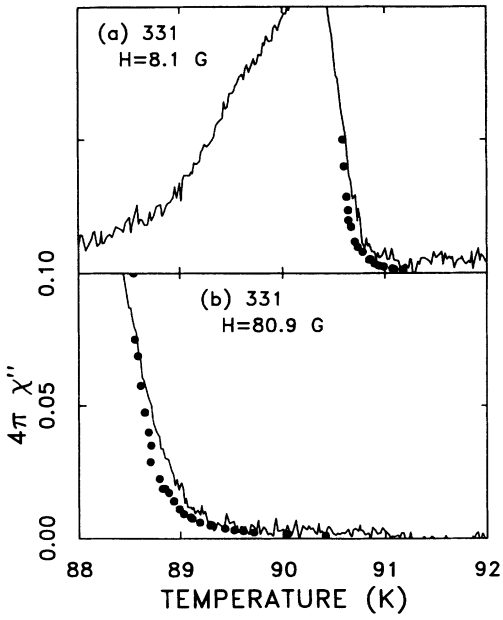

FIG. 11. χ'' vs T as measured directly (solid line) and as calculated (symbols) from ρ_L measurements. (a) Sample 331 and $H=8.1$ G. (b) Sample 331 and $H=80.9$ G. The vertical scales are the same in (a) and (b).

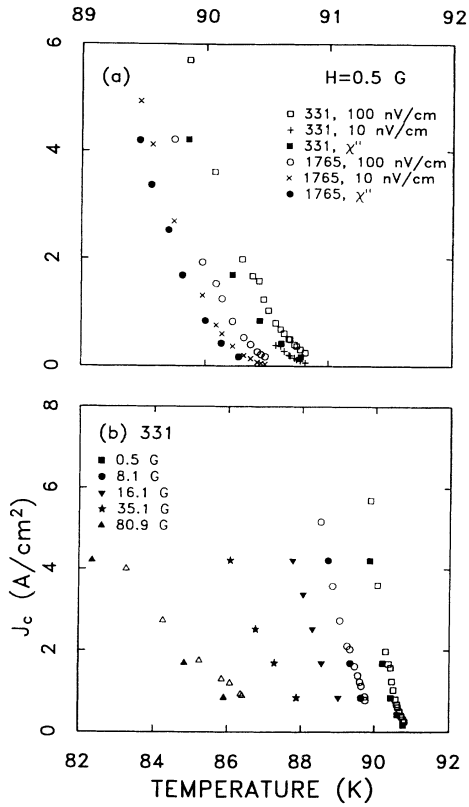

FIG. 12. J_c vs T as determined from I-V measurements and from χ_m'' measurements. (a) samples 331 and 1765 with $H=0.5$, 8.1, and 80.9 G. In (b), the open symbols for $H=0.5$, 8.1, and 80.9 G represent J_c determined from I-V measurements using a 100-nV/cm electric-field criterion.

measurements from Refs. 16 and 17. Figure 10 shows results for samples 331, 1765 at $H=0.5$ G and Fig. 11 shows data for sample 331 at $H=8.1$ and 80.9 G. The skin depth approximation agrees with directly measured χ'' in both samples. Differences between calculated and measured χ'' may result from sample inhomogeneity. For inhomogeneous materials, transport measurements may underestimate the "average" resistivity of the sample as determined by a χ'' measurement, since χ'' is less likely to be dominated by small regions of the sample.

Close to but above T_c, the I-V characteristics are nonlinear except for very small current densities and the model of a normal metal skin depth effect is no longer appropriate. For $T\approx T_c$, we observed $V\propto I^a$ with $a\approx 2$ for more than three decades in voltage. Below T_c I-V characteristics are consistent with a well-defined critical current, and J_c was determined for selected temperatures. It is also possible to extract J_c data from χ'' data using critical-state models.[7] Since all of our measurements were done for relatively small excitation fields, $H_{ac}<0.5$ G, J_c should be virtually independent of H_{ac} and the conditions for the Bean critical-state model should be well met.[7,22] The Bean model predicts that $4\pi\chi_m''=0.21$, where χ_m'' is the maximum value of χ''. For samples 331 and 1765, the magnitude of $4\pi\chi_m''\approx 0.15$ and 0.20, respectively, are in reasonable agreement with the Bean model prediction. Lower values are consistent with expectations for granular superconductors and result from intragranular flux expulsion.[7]

The Bean model predicts a relationship between J_c at the temperature for which χ'' is maximum (T_p), the sample radius R, and H_{ac},[3]

$$J_c(T_p)=H_{ac}/R \ . \tag{5}$$

We next compare J_c as determined using Eq. (5) with J_c obtained directly from I-V measurements. Figure 12(a) shows plots of J_c as determined from χ_m'' and directly taken from the I-V data for samples 331 and 1765 at $H=0.5$ G. Figure 12(b) shows J_c as determined from χ_m'' and directly taken from the I-V data for sample 331 at $H=0.5$, 8.1, and 80.9 G. Two sets of J_c from I-V data are shown in Fig. 12(a), one determined using a 0.1-μV/cm and the other form a 10-nV/cm electric-field criterion. The agreement between Bean model predictions and I-V measurements is good.

VI. CONCLUSION

We have performed extensive $\chi_{ac}(T)$ measurements for selected magnetic fields $0.5\le H\le 80.9$, excitation fields $1\le H_{ac}\le 450$ mG, and $80\lesssim T\lesssim 93$ K on a set of sintered YBCO samples. At $H_{ac}\gtrsim 90$ mG, we observe χ_{ac} behavior that is consistent with critical-state models and similar to numerous other studies. The measurements for $H_{ac}\lesssim 90$ mG represent the first extensive χ_{ac} measurements in this small H_{ac} regime for sintered YBCO. We observe a distinct and qualitatively different χ'' behavior for $H_{ac}\lesssim 9$ mG, and see a crossover between the two regimes for $9\lesssim H_{ac}\lesssim 90$ mG. Based on these observations, we have determined the threshold field for the breakdown of the critical-state model; $H_{ac}^t\sim 90$ mG for two samples with $\langle d_g\rangle\approx 6$ μm and $H_{ac}^t\sim 45$ mG for the sample with $\langle d_g\rangle\approx 12$ μm. These results are consistent with predictions based on a Josephson-array model and the morphology of our samples.

We have additionally characterized the behavior of $\chi''(T)$ in this small H_{ac} regime, both for different samples and as a function of magnetic field strength in the range $0.1\le H\le 81$ G. We find that for very small H_{ac}, χ'' differs from its behavior at large H_{ac} by having significantly smaller peak values and by having a $\chi''(T)$ shape that is independent of H_{ac}. The shape at small H_{ac} exhibits a sample-dependent structure that is not observable in the critical-state regime ($H_{ac}\gtrsim 90$ mG).

*Current address: Physics Department, Trinity College, Hartford, CT 06106.

[1]H. Küpfer, I. Apfelstedt, W. Schauer, R. Flükiger, R. Meier-Hirmer, and H. Wühl, Z. Phys. B **69**, 159 (1987).
[2]J. R. Clem, Physica C **153-155**, 50 (1988).
[3]S. D. Murphy, K. Renouard, R. Crittenden, and S. M. Baghat, Solid State Commun. **69**, 367 (1989).
[4]M. Nikolo and R. F. Goldfarb, Phys. Rev. B **39**, 6615 (1989).
[5]Z. Koziol, Physica C **159**, 281 (1989).
[6]K.-H. Müller, Physica C **159**, 717 (1989).

[7]S. Senoussi, J. Phys. III **2**, 1041 (1992).
[8]A. M. Campbell, J. Phys. C **2**, 1492 (1969); **4**, 3186 (1971).
[9]A. Houghton and M. A. Moore, Phys. Rev. B **38**, 5045 (1988).
[10]Y. Shih, C. Ebner, and D. Stroud, Phys. Rev. B **30**, 134 (1984); C. Ebner and D. Stroud, *ibid.* **31**, 165 (1985).
[11]B. D. Josephson, Phys. Lett. **1**, 251 (1962).
[12]T. van Duzer and C. W. Turner, *Principles of Superconducting Devices and Circuits* (Elsevier, New York, 1981).
[13]L. Krusin-Elbaum, A. P. Malezemoff, Y. Teshurin, D. C. Cronemeyer, and F. Holtzberg, Physica C **153-155**, 1469 (1988).
[14]M. S. Rzchowski, S. P. Benz, M. Tinkham, and C. J. Lobb, Phys. Rev. B **42**, 2041 (1990); S. P. Benz, M. S. Rzchowski, M. Tinkham, and C. J. Lobb, *ibid.* **42**, 2041 (1990).
[15]CTI-Cryogenics model 22 cold head.
[16]W. M. Tiernan and R. B. Hallock, Phys. Rev. B **48**, 3423 (1992).
[17]W. M. Tiernan, Ph.D. dissertation, University of Massachusetts at Amherst, 1992.
[18]J. C. W. Chien, B. M. Gong, Y. S. Yang, J. M. Madsen, W. M. Tiernan, and R. B. Hallock, Physica C **165**, 279 (1990).
[19]J. C. W. Chien, B. M. Gong, J. M. Madsen, and R. B. Hallock, Phys. Rev. B **38**, 853 (1988).
[20]J. C. W. Chien, B. M. Gong, X. Mu, and Y. S. Yang, J. Polym. Sci. A **28**, 1999 (1990).
[21]J. R. Clem, in *Magnetic Susceptibility of Superconductors and Other Spin Systems,* edited by R. A. Hein, T. L. Francavilla, and D. H. Liebenberg (Plenum, New York, 1992).
[22]C. P. Bean, Rev. Mod. Phys. **36**, 31 (1964).

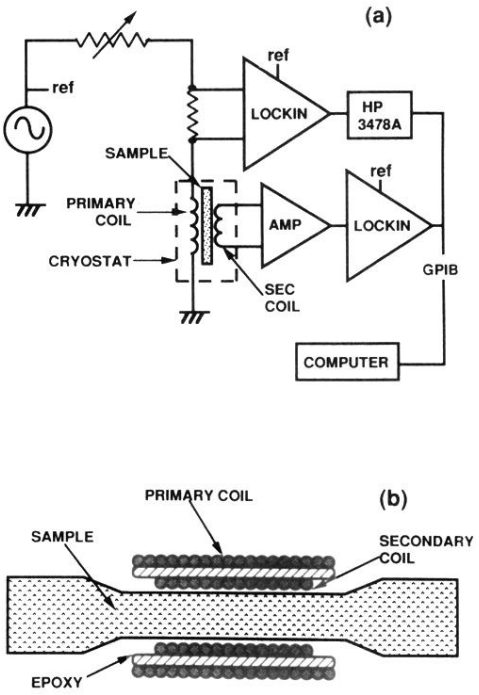

FIG. 1. (a) Schematic of circuit used for χ_{ac} measurements. (b) Sectional view along length of a typical sample.